7-1-2012

Performance Mapping for Variable Ductless Heat Pump Systems in Heating, Cooling and Defrost Operation

Howard Cheung
Ray W. Herrick Laboratories, Purdue University, cheung@purdue.edu

James E. Braun
Ray W. Herrick Laboratories, Purdue University

Performance Mapping for Variable Ductless Heat Pump Systems in Heating, Cooling and Defrost Operation

Howard CHEUNG*, James E. BRAUN

Ray W. Herrick Laboratories, School of Mechanical Engineering, Purdue University
West Lafayette, Indiana, U.S.A
E-mail: cheung@purdue.edu and jbraun@purdue.edu

* Corresponding Author

ABSTRACT

As the market for ductless heat pump systems (DHPs) has grown so has the need to represent their performance in building simulation programs to enable the study of their effect on building energy consumption and to assist in the building design. For computationally efficient building assessments, quick computation for power consumption under different external effects is necessary. In this paper, data from various heating and cooling tests on a 9500 Btu/h (2782 W) unit are presented. In both operation modes, the minimum and maximum capacity under different environmental conditions, the indoor unit power consumption and the part-load performance were modeled from the data. A defrost model was also constructed to adjust the heating part-load model for defrost operation and a sensible heat ratio model was built to capture the humidity removal performance of the DHP in cooling. Good agreement between the measurement and prediction was found.

1. INTRODUCTION

In spite of the widespread use of ductless heat pump systems (DHPs) in Asia and Europe, the market for DHPs in the U.S. has just started to grow in recent years. While these units feature the use of variable speed drives and electronic expansion valves for good part-load performance, these characteristics complicate the modeling of their performance. To analyze these units for energy-efficient building designs, building simulation programs require a computational efficient model of DHPs.

Computational efficient models for building simulations are usually provided as empirical models constructed from experimental data. A polynomial and bypass factor model was provided from experimental data for direct expansion coils (Brandemuehl et. al 1993). A similar model for heat pumps was also generated from experimental data on packaged units (Mercer 2003). A model for variable speed drive split systems was also made for EnergyPlus (Zhou et al 2008). Further development of direct expansion coil models was based on a generic rating-data-based method (Yang and Li 2010). DHP models in heating and cooling mode were also developed for a two different units (Ecotope Inc. 2011). However, these papers did not account for some common control strategies that adjust maximum compressor speed based on ambient temperature and the effect of defrost operation on the performance, which are addressed in this paper.

The models presented in this paper were constructed based on testing data for heating and cooling mode obtained from a 2782W (9,500 Btu/h) DHP installed within psychrometric chambers. A model of power consumption was built based on the capacities of the unit and the airflows under different environmental conditions for both heating and cooling operation. A sensible heat ratio model was also developed for cooling mode and a defrost adjustment model was made for heating mode.

2. EXPERIMENTAL SET-UP AND PROCEDURE

The DHP experiments were carried out in psychrometric chambers having indoor and outdoor rooms. Figure 1 shows the refrigerant circuit for the experimental set-up. The refrigerant pipe length between the indoor and the outdoor unit was 11m and the system was charged with 1.05 kg of refrigerant R410A.

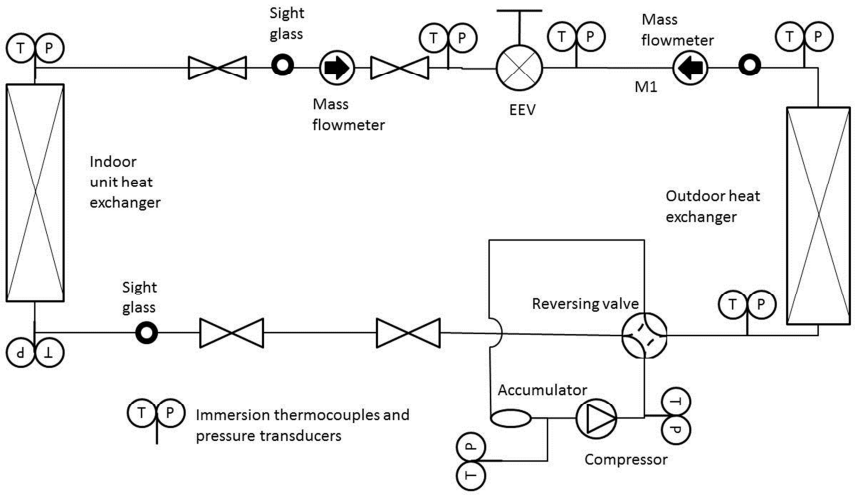

Figure 1: Schematic of the refrigerant circuit of the experimental set-up.

T-type thermocouples immersed in the refrigerant and pressure transducers with accuracy ±0.25% were installed along the refrigerant side circuit in Figure 1. Refrigerant mass flows were also measured using two Coriolis mass flowmeters. Eight T-type thermocouples were installed at the air outlet of the indoor unit and nine thermocouples of the same type were installed at the air inlets for each heat exchanger to measure the air-side dry-bulb temperature. The humidity condition of air was measured using chilled mirror dewpoint sensors with accuracy ±0.2°C. The airflow across the indoor unit was measured with nozzles air-ducted downstream to the indoor unit according to the ASHRAE Standard 41.2 with accuracy ±1.0%. Power meters were installed to measure the power consumption of the outdoor unit and the indoor unit at an accuracy of ±0.2%. Compressor rotational frequency was also acquired by mounting an accelerometer on the compressor surface connected in series with an amplifier and using an analog signal analyzer.

Steady state data were obtained in experiments with different environmental conditions, airflows and room temperature setpoints that led to a variety of expansion valve openings and compressor speeds. Under conditions where it was possible to achieve a stable control of compressor speed and expansion valve opening, steady state data were obtained by averaging data over ten minutes of operation. If continuous non-periodic variations were found after three hours of operation, the last hour of data were averaged for steady state data. For defrost operations, the analysis was conducted on data obtained in the second cycle of operation after startup.

Thirty-two steady state heating tests and thirty-six steady state cooling tests were carried out. Thirteen other heating tests with defrost operation were also conducted. The range of conditions of these tests is shown in Table 1 and Table 2.

Table 1: Range of conditions for heating tests (defrost cases included).

Outdoor dry-bulb temperature [°C]	Outdoor wet-bulb temperature [°C]	Airflow [m^3/h]	Average compressor speed achieved [Hz]	Indoor dry-bulb temperature [°C]
-13.87 ~ 16.70	-15.34 ~ 9.27	247 ~ 389	40.5 ~ 94.3	17.69 ~ 24.49

Table 2: Range of conditions for cooling tests.

Outdoor dry-bulb temperature [°C]	Airflow [m^3/h]	Average compressor speed achieved [Hz]	Indoor dry-bulb temperature [°C]	Indoor wet-bulb temperature [°C]
19.36 ~ 46.16	210 ~ 408	43.3 ~ 68.4	23.17 ~ 26.82	12.57 ~ 19.60

3. EMPIRICAL MODELING APPROACH AND RESULTS

3.1 Minimum capacity model

To map part-load performance, maximum and minimum capacity were defined at different environmental conditions in order to bound and normalize part-load performance. The minimum capacity equations for heating are given as equation (1) and (2).

$$\dot{Q}_{min,heating} = a_0 + a_1 T_{amb,dry} + a_2 T_{in,dry} \tag{1}$$

$$\dot{W}_{min,heating} = a_3 + a_4 T_{amb,dry} + a_5 T_{in,dry} \tag{2}$$

The minimum capacity equations for cooling are given in equation (3). Indoor wet-bulb temperature is an input to the model to account for conditions where condensation is occurring on the coil. The value of the wet-bulb temperature used in the model depends on the estimated sensible heat ratio (SHR) discussed in a later section. When the coil is wet (SHR < 1), the actual indoor wet-bulb temperature is used. However, when the coil is dry, an effective wet-bulb temperature that gives SHR = 1 is estimated using equation (16) and used in equation (3).

$$\begin{aligned} \dot{Q}_{min,cooling} \text{ or } \dot{W}_{min,cooling} &= f_1(T_{amb,dry}) f_2(T_{in,wet}) \\ f_1(T_{amb,dry}) &= \begin{cases} a_6 + a_7 T_{amb,dry} & \text{if } T_{amb,dry} > 27.7°C \\ a_8 + a_9 T_{amb,dry} & \text{otherwise} \end{cases} \\ f_2(T_{in,wet}) &= 1 + a_{10}(T_{in,wet} - 19.4°C) \end{aligned} \tag{3}$$

While the coefficients in equations (1) and (2) were obtained by linear regression, the coefficients in equation (3) were obtained by constrained minimization on the cooling capacity to ensure the continuity of f_1 in equation (3) at $T_{amb,dry}$ 27.7°C. The disjoint in f_1 in equation (3) was determined by the outdoor temperature where the minimum compressor speed changed. Due to a change in control strategy, it was observed that the minimum cooling capacity increased with outdoor dry-bulb temperature when the outdoor dry-bulb temperature was lower than 27.7°C, and increased when the outdoor temperature was above 27.7°C. The results of the minimum capacity models appear in Figure 2 and Figure 3 and the coefficients are listed in the appendix.

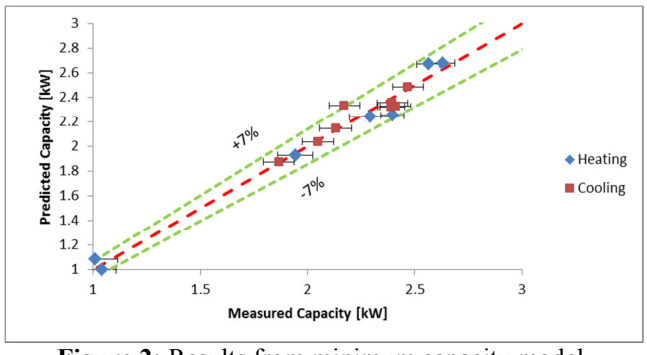

Figure 2: Results from minimum capacity model.

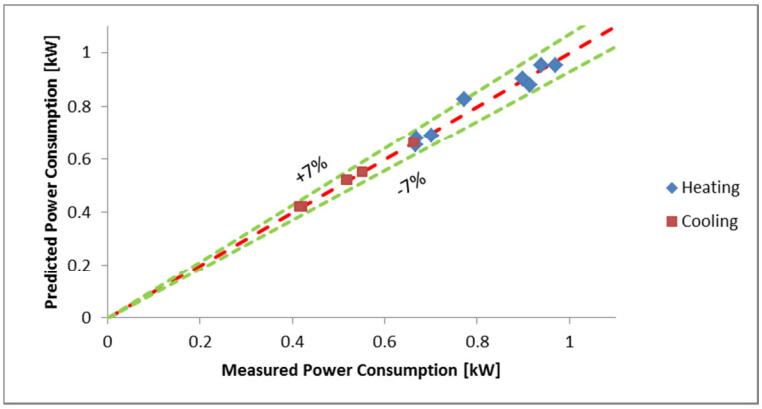

Figure 3: Results from outdoor power consumption model at minimum capacity.

3.2 Maximum capacity model

To completely describe the boundary, the maximum capacity performance is modeled in a manner similar to the minimum capacity using equations (4), (5) and (6) for heating and equation (7) for cooling.

$$\dot{Q}_{max,heating} \text{ or } \dot{W}_{max,heating} = f_3(T_{amb,dry}) f_4(T_{in,dry}) \tag{4}$$

$$f_3(T_{amb,dry}) = \begin{cases} b_0 + b_1 T_{amb,dry} & \text{if } T_{amb,dry} > 8.33°C \\ b_2 + b_3 T_{amb,dry} & \text{if } 8.33°C \geq T_{amb,dry} > -2.78°C \\ b_4 + b_5 T_{amb,dry} & \text{otherwise} \end{cases} \tag{5}$$

$$f_4(T_{in,dry}) = 1 + b_6(T_{in,dry} - 21.1°C) \tag{6}$$

$$\begin{aligned} &\dot{Q}_{max,cooling} \text{ or } \dot{W}_{max,cooling} = f_5(T_{amb}) f_6(T_{in,wet}) f_7(\dot{V}) \\ &f_5(T_{amb,dry}) = \begin{cases} b_7 + b_8 T_{amb,dry} + b_9 T_{amb,dry}^2 & \text{if } T_{amb,dry} > 27.7°C \\ b_{10} + b_{11} T_{amb,dry} & \text{otherwise} \end{cases} \\ &f_6(T_{in,wet}) = 1 + b_{12}(T_{in,wet} - 19.4°C) + b_{13}(T_{in,wet} - 19.4°C)^2 \\ &f_7(\dot{V}_{air}) = 1 + b_{14}(\dot{V} - 380 m^3/h) \end{aligned} \tag{7}$$

Since experimental results suggest that the maximum compressor frequency changes with the ambient temperature, disjoints of piecewise functions in equation (5) and f_5 in equation (7) are used to explain the changes. In heating, the maximum compressor frequency is found to be increasing as ambient temperature decreases from 8.33°C to -2.78°C but remains unchanged at the other temperatures. In cooling, the maximum compressor speed is found to be lower when the ambient temperature drops below 27.7°C. As different airflows were measured in maximum cooling capacity tests, an adjustment factor for airflow is added to equation (7). As described for the minimum capacity model, the wet-bulb temperature used in the equation 7 is the indoor condition when the coil is wet and an effective value that gives SHR=1 when the coil dry.

The coefficients in equations (4) to (7)were also estimated by constrained minimization on the capacity and power consumption to ensure the continuity of functions in equations (5) and (7). Results are plotted in Figure 4 and Figure 5.

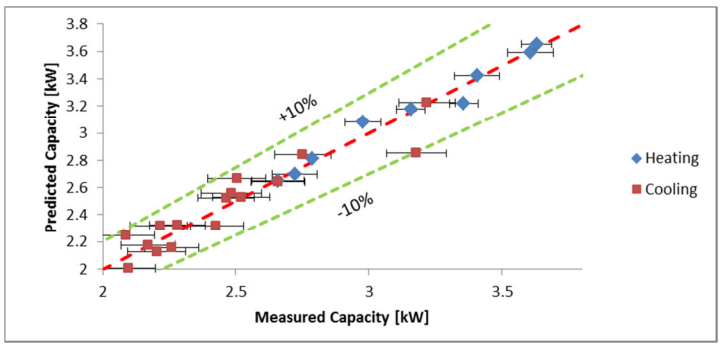

Figure 4: Results from maximum capacity model.

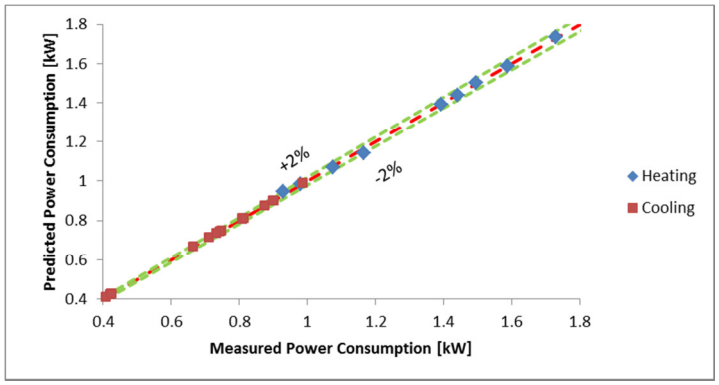

Figure 5: Results from outdoor unit power consumption model at maximum capacity.

3.3 Part-load model

The part-load performance model for heating and cooling operation is given in equation (8).

$$w_f = D_0 q_f + D_1 v_f + D_2 q_f v_f + D_3 q_f^2$$

$$w_f = \frac{\dot{W} - \dot{W}_{min}}{\dot{W}_{max} - \dot{W}_{min}}$$

$$q_f = \frac{\dot{Q} - \dot{Q}_{min}}{\dot{Q}_{max} - \dot{Q}_{min}} \tag{8}$$

$$v_f = \frac{\dot{V} - \dot{V}_{min}}{\dot{V}_{max} - \dot{V}_{min}}$$

The coefficients in equation (8) are obtained by constrained optimization to minimize the difference between the estimated and measured outdoor unit power consumptions. Constraints listed in equations (9) and (10) are used to ensure the correct estimation of power consumption at the minimum and maximum capacity and that the power consumption is decreasing with the capacity.

$$\Sigma D_i = 1 \tag{9}$$

$$\frac{\partial w_f}{\partial q_f} = D_0 + D_2 + 2D_3 q_f \geq 0 \tag{10}$$

The applicable range of equation (8) can be defined by the data used for model construction as tabulated in Table 3 and Table 4. Since only three indoor flow settings are available, all the airflows shown in Table 3 and Table 4 are the average airflows from tests under the same indoor flow setting.

Table 3: Data range for equation (8) in heating operation.

Airflow [m^3/h]	388	315	249
Dimensionless capacity q_f in equation (8)	0.091 ~ 1	-0.161 ~ 0.931	0 ~ 0.399

Table 4: Data range for equation (8) in cooling operation.

Airflow [m^3/h]	380	314	244
Dimensionless capacity q_f in equation (8)	0.093 ~ 1	0.036 ~ 1.25	0 ~ 0.57

Results of the estimation are shown in Figure 6.

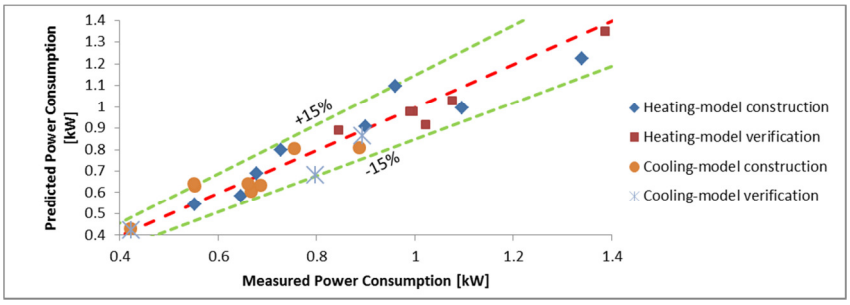

Figure 6: Results from part-load model.

3.4 Indoor unit power consumption model

The indoor unit power consumption was found to have a linear relationship with the indoor airflow as shown in equation (11) and the parameters were estimated with linear regression. Figure 7 illustrates the accuracy of the correlation.

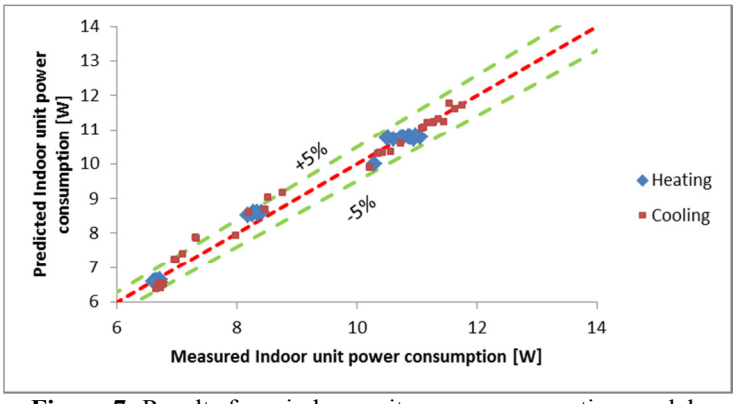

Figure 7: Results from indoor unit power consumption model.

$$\dot{P}_{heating} \text{ or } \dot{P}_{cooling} = c_0 + c_1 \dot{V} \tag{11}$$

3.5 Defrost model

To account for the effect of defrost in heating operation, adjustment factors were made on the part-load model in equation (8). Since significant defrost operation (decrease in COP larger than 1.5%) was only found when the ambient temperature was less than or equal to -2.78°C, only data with ambient temperature below -2.78°C were used to build the model. One factor is the estimation of defrost time because the indoor fan will be switched off when the

unit is in defrost. The other factor is the power consumption because extra power is used to defrost the unit without heating up the indoor environment. Equations (12) and (13) are used to account for the defrost operation.

$$\%\ \text{increase in power consumption} = p_0 + p_1 T_{amb,dry} + p_2 \frac{\dot{V}}{\dot{V}_{max}} + p_3 \frac{\dot{Q}}{\dot{W}} \frac{\dot{V}}{\dot{V}_{max}} \quad (12)$$

$$\frac{\text{Defrost Time}}{\text{Overall Cycle Time}} = p_4 + p_5 T_{amb,dry} + p_6 \frac{\dot{Q} - \dot{Q}_{min}}{\dot{Q}_{max} - \dot{Q}_{min}} \quad (13)$$

Results from equations (12) and (13) are plotted in Figure 8 and Figure 9.

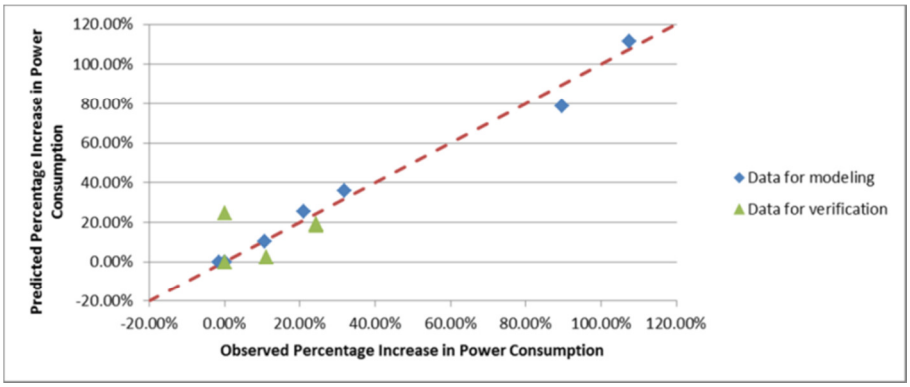

Figure 8: Results from equation (12).

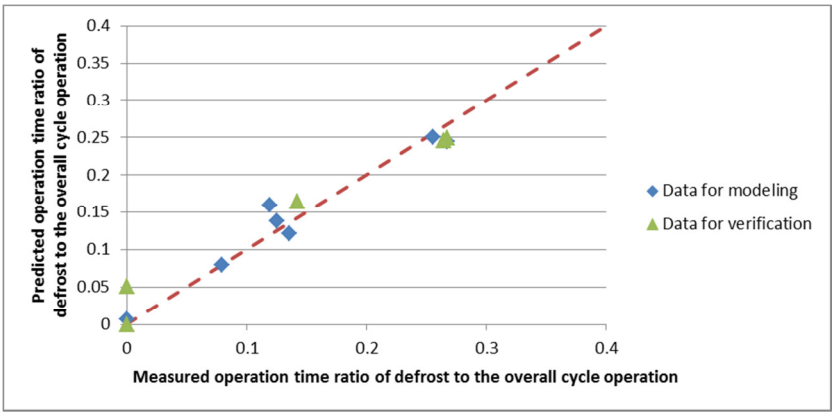

Figure 9: Results from equation (13).

3.6 Sensible heat ratio model

Cooling operation also removes humidity from the indoor room and the effect can be accounted for using a bypass factor model presented in Brandemuehl *et. al* (1993). The model is given in equations (14), (15) and (16).

$$BF_{rated} = \frac{h_{out} - h_{adp}}{h_{in} - h_{adp}} \quad (14)$$

$$\omega_{adp} = \omega(h = h_{adp}, r = 1) \quad (15)$$

$$SHR = min\left(\frac{h(T{=}T_{in,dry}, \omega{=}\omega_{adp}}{h_{in} - h_{adp}}, 1\right) \quad (16)$$

A rated bypass factor is found from the results observed with ambient temperature 35°C, indoor dry-bulb temperature 26.7°C, indoor wet-bulb temperature 19.4°C and 380m^3/h. The results of the model are plotted in Figure 10.

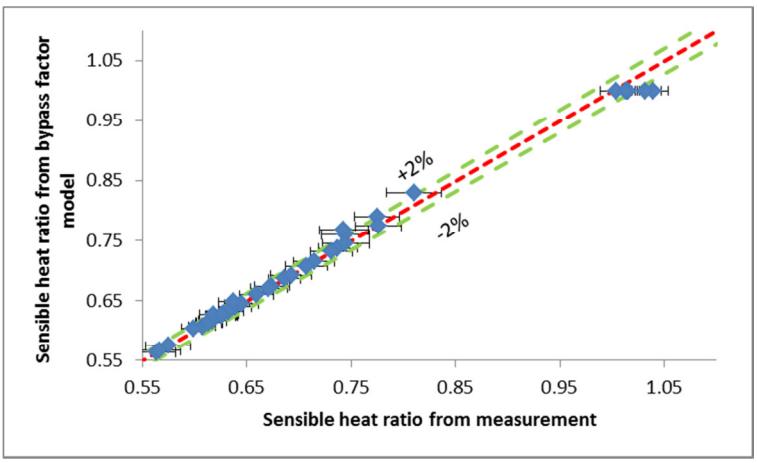

Figure 10: Results from bypass factor model.

4. CONCLUSIONS

The paper presents a method for modeling the performance of a DHP having a variable speed compressor and fans. The model captures minimum and maximum capacity performance, part-load performance, humidity removal ability and the effect of defrost on performance. Data were collected in psychrometric chambers with different environmental conditions, compressor speeds and indoor fan speeds. Equations with piecewise functions were introduced to account for the environmental effect on the control strategy of the compressor speed, outdoor fan speed and electronic valve opening. Mapping of the performance was conducted using linear regression, constrained optimization and bypass factor model. Results show that the model can predict the sensible heat ratio, the defrost operation effect, the maximum capacity and minimum capacity accurately but improvements are needed to explain the effect of control on performance during part-load operation.

NOMENCLATURE

a, b, c, D, p	regression coefficients	(--)	**Subscripts**	
h	air-water enthalpy	(kJ/kg)	adp	coil surface
ω	humidity ratio	(kg/kg)	amb	ambient
Ṗ	indoor unit power consumption	(W)	cooling	cooling operation
Q̇	capacity	(kW)	dry	dry-bulb
r	relative humidity	(--)	heating	heating operation
SHR	sensible heat ratio	(--)	in	indoor
T	temperature	(°C)	max	maximum
V	indoor unit airflow	(m^3/h)	min	minimum
Ẇ	outdoor unit power consumption	(kW)	wet	wet-bulb

REFERENCES

ASHRAE Standard 41.2-1987 (RA 92), Standard Methods for Laboratory Airflow Measurement. (1992). Atlanta, GA: American Society of Heating, Refrigerating and Air-Conditioning Engineers, Inc.

Brandemuehl, M. J., Gabel, S. and Andresen, I. (1993). *HVAC 2 Toolkit: A Toolkit For Secondary HVAC System Energy Calculations*. Atlanta, GA: American Society of Heating, Refrigerating and Air-Conditioning Engineers, Inc.

Ecotope Inc. (2011) *Ductless Heat Pump Impact & Process Evaluation: Lab-Testing Report (E11-225)*, Retrieved from Northwest Energy Efficiency Alliance Website: http://neea.org/research/reports/E11-225-DHP-Lab-Testing.pdf

Mercer, K. (2003). *Modeling And Testing Strategies For Evaluating Ventilation Load Reduction Technologies*. (Master Thesis). Ray W. Herrick Laboratories, West Lafayette, IN.

Yang, H. and Li, H. (2010). A Generic Rating-Data-Based (GRDB) DX Coils Modeling Method, *HVAC&R Research*, 16 (3), 331 – 353

Zhou, Y. P., Wu, J. Y., Wang, R. Z., Shiochi, S. and Li, Y. M. (2008). Simulation And Experimental Validation of the Variable-refrigerant-volume (VRV) air-conditioning system in EnergyPlus. *Energy and Buildings*, 40, 1041 - 1047

ACKNOWLEDGEMENT

The authors acknowledge Ecotope Inc. for funding the development of the project and graduate research assistant Simbarashe Nyika for helping to set up and operate the experiments.

APPENDIX: VALUES OF COEFFICIENTS

Table A.1: Values of coefficients of Equations

a_0 [kW]	1.8106	$\dot{Q}$ model		$\dot{Q}$ model		$\dot{W}$ model	
a_1 [kW/K]	0.0546	a_6 [kW]	3.8063	b_0 [kW]	2.6460	b_0 [kW]	0.8550
a_2 [kW/K]	-0.0013	a_7 [kW/K]	-0.0476	b_1 [kW/K]	0.0518	b_1 [kW/K]	0.0104
a_3 [kW]	0.6609	a_8 [kW]	1.9666	b_2 [kW]	3.5119	b_2 [kW]	1.5385
a_4 [kW/K]	0.0094	a_9 [kW/K]	0.0188	b_3 [kW/K]	-0.0521	b_3 [kW/K]	-0.0716
a_5 [kW/K]	0.0066	a_{10} [/K]	0.0079	b_4 [kW]	3.8977	b_4 [kW]	1.8129
		$\dot{W}$ model		b_5 [kW/K]	0.0867	b_5 [kW/K]	0.0271
		a_6 [kW]	0.2054	b_6	-0.0074	b_6	0.0000
		a_7 [kW/K]	0.0113	b_7 [kW]	6.8078	b_7 [kW]	0.4056
		a_8 [kW]	0.1835	b_8 [kW/K]	-0.1903	b_8 [kW/K]	0.0076
		a_9 [kW/K]	0.0121	b_9 [kW/K^2]	0.0020	b_9 [kW/K^2]	0.0001
		a_{10} [/K]	0.0000	b_{10} [kW]	0.3817	b_{10} [kW]	-0.2360
				b_{11} [kW/K]	0.0975	b_{11} [kW/K]	0.0340
				b_{12} [/K]	0.0355	b_{12} [/K]	0.0000
				b_{13} [/K^2]	0.0020	b_{13} [/K^2]	0.0000
				b_{14} [/(m^3/h)]	0.0018	b_{14} [/(m^3/h)]	0.0000

Table A.2: Values of coefficients of Equations (continued).

Heating		Heating		p_0	0.3967
D_0	1.1588	c_0 [W]	-0.9302	p_1 [/K]	-0.0480
D_1	-0.2693	c_1 [W/(m^3/h)]	0.0301	p_2	-2.1182
D_2	-1.4304	Cooling		p_3	0.7052
D_3	1.5409	c_0	-1.3154	p_4 [/K]	0.0263
Cooling		c_1 [W/(m^3/h)]	0.0321	p_5	-0.0132
D_0	0.9926			p_6	-0.1557
D_1	-0.2836			BF_{rated}	0.00
D_2	0.4650				
D_3	-0.1740				